Journal of Alloys and Compounds 647 (2015) 756–762

Contents lists available at ScienceDirect

Journal of Alloys and Compounds

journal homepage: http://www.elsevier.com/locate/jalcom

Improved hydrogen storage properties of $LiAlH_4$ by mechanical milling with TiF_3

Lei Zang, Jiaxing Cai, Lipeng Zhao, Wenhong Gao, Jian Liu*, Yijing Wang

Institute of New Energy Material Chemistry, Key Laboratory of Advanced Energy Materials Chemistry (MOE), Tianjin Key Lab of Metal, Nankai University, 94 Weijin Road, Tianjin 300071, China

ARTICLE INFO

Article history:
Received 23 March 2015
Received in revised form
2 June 2015
Accepted 4 June 2015
Available online 10 June 2015

Keywords:
Hydrogen storage materials
Energy storage
Complex hydride
$LiAlH_4$
TiF_3
Ball milling

ABSTRACT

Dehydrogenation behavior of $LiAlH_4$ (lithium alanate) admixed with TiF_3 is investigated by pressure-composition-temperature (PCT), fourier transform infrared spectroscopy (FTIR), X-ray Diffraction (XRD), differential scanning calorimetry (DSC) and temperature programmed desorption (TPD). The TiF_3 addition enhances kinetics of $LiAlH_4$ and decreases the decomposition temperature. The $LiAlH_4$-2 mol % TiF_3 sample starts to release hydrogen at about 35 °C and the dehydrogenation rate reaches a maximum value at 108.4 °C, compared with 145 °C and 179.9 °C for the as-received $LiAlH_4$. As for the dehydrogenation kinetics, the $LiAlH_4$-2 mol % TiF_3 sample releases about 7.0 wt % H_2 at 140 °C within 80 min. In comparison, the as-received $LiAlH_4$ sample releases only 0.8 wt % hydrogen under the same conditions. The existence of proposed catalyst, Al_3Ti formed in-situ in the process of dehydrogenation, has been confirmed experimentally by XRD measurements. The activation energy of $LiAlH_4$-2 mol % TiF_3 composite is deduced to be 66.76 kJ mol^{-1} and 88.21 kJ mol^{-1} for the first and second reaction stages of $LiAlH_4$ dehydrogenation.

1. Introduction

With the rapid global economic development, the fossil energy is in an accelerating pace towards exhaustion. CO_2 and other harmful gases from the burning of fossil fuels, can lead to the global warming and environmental pollution problem. In order to solve these problems, many countries around the world are positively developing renewable energy and clean energy. Hydrogen is an ideal energy carrier due to its storability, environmental friendliness, high calorific value and cost effectiveness [1,2]. Hydrogen generation and storage are considered as one of the main problems which have to be solved in the future development of hydrogen technology [3–11]. It is crucial to find new applicable hydrogen storage materials with high performances. Solid state hydrogen storage materials have large volume density, good safety performance, ease of use and transportation advantages. Therefore, future research will focus on the safety of hydrogen storage and development of new solid hydrogen storage materials with high-performance [12]. According to the goal of DOE for 2015, the target of hydrogen capacity is 6.5 wt. % [13].

In recent years, light weight complex hydrides are receiving increasing attention owing to their high gravimetric and volumetric hydrogen capacities [14]. Among them, $LiAlH_4$ is regarded as one of the most promising hydrogen storage materials owing to its high theoretical hydrogen storage capacity (10.5 wt %). $LiAlH_4$ material has the following advantages: higher theoretical hydrogen storage capacity; lower decomposition reaction enthalpy change, which lets it release hydrogen at relatively low temperature [15]. Dehydrogenation of $LiAlH_4$ occurs as given in the following reaction:

$$3LiAlH_4 \rightarrow Li_3AlHl_6 + 2Al + 3H_2 \quad (5.3\ wt\ \%\ H_2) \qquad R1$$

$$Li_3AlH_6 \rightarrow 3LiH + Al + 1.5H_2 \quad (2.6\ wt\ \%\ H_2) \qquad R2$$

$$LiH + Al \rightarrow LiAl + 1.5H_2 \quad (2.6\ wt\ \%\ H_2) \qquad R3$$

It releases 5.3 wt % H_2 in the first step at 150 °C–175 °C, and in the second step it releases 2.6 wt % H_2 at 180 °C–220 °C [16–18]. The whole process of R3 only occurs in vacuum and releases 2.6 wt % H_2 at above 400 °C, which is considered to be unsuited for various applications. Thus, it is commonly accepted that only the first two desorption processes of $LiAlH_4$ are considered. However, there are also many disadvantages for $LiAlH_4$ material, such as: extremely

* Corresponding author.
E-mail address: liujian@nankai.eud.cn (J. Liu).

http://dx.doi.org/10.1016/j.jallcom.2015.06.036
0925-8388/

high plateau pressure at relatively low temperatures, which makes the hydride practically irreversible; the presence of an exothermic decomposition reaction [15]. In addition, the hydrogen release rate is relatively slow, which can be improved by ball milling and doping. At present, a lot of research has been carried out on doping modification. $LiAlH_4$ starts to decompose at 61 °C with 3 mol % $NiFe_2O_4$ as an additive and releases 7.2 wt % H_2 at 180 °C [19]. Balema et al. mechanically ball milled $LiAlH_4$-3 mol % $TiCl_4$ at room temperature for 5 min, and then $LiAlH_4$ has completely broken down to Li_3AlH_6, Al and H_2 [20]. So far, the reported catalysts for $LiAlH_4$ are as given in the following: (1) metal hydrides, such as MgH_2 [21]; (2) elemental metals, such as Al [22], Ti [23], Fe [24], Ni [25], and Sc [23]; (3) metal halides, such asVCl_3 [26] and [27], TiF_3 [28], $TiCl_3$ [29,32] and $TiCl_4$ [20] and [30]; (4) alloys, such as $TiAl_3$ and Ti_3Al [23]; (5) metal oxides, such as Nb_2O_5 and Cr_2O_3 [31], Fe_2O_3 and Co_2O_3 [29,32]; and (6) others, such as TiC and TiN [33], graphite [34], $MnFe_2O_4$ [35] and MWCNTs [36].

However, the catalytic mechanism of TiF_3 on $LiAlH_4$ is still an unsolved problem. It is thought that TiF_3 reacts with $LiAlH_4$ to form Al_3Ti [28], and Al_3Ti is considered to be an effective catalyst for the dehydrogenation of $LiAlH_4$ [22]. The formation of nano/micro-crystalline Al_3Ti in the milling process of 4:1 $LiAlH_4/TiCl_4$ and 3:1 $NaAlH_4/TiCl_3$ mixtures has been reported by Balema et al. [37] and Majzoub et al. [38]. but Al_3Ti cannot be detected experimentally for samples of a typical doping level <5 mol %. To our best knowledge, there is no report on the in-situ formation of Al_3Ti during the process of dehydrogenation. However, another mechanism of fluoride substitution has been reported for Na_3AlH_6 and $NaBH_4$ [39–41]. Fluorine partially substitutes hydrogen to form $Na_3AlH_{6-x}F_x$ and $NaBH_{4-x}F_x$. It may lead to destabilization, which tends to facilitate hydrogen desorption. In the present work, TiF_3 (1, 2, 4, 6 mol %)-$LiAlH_4$ have been ball milled under certain conditions. Samples have been analyzed by Pressure–composition– temperature (PCT) apparatus, differential scanning calorimetry (DSC), X-ray diffraction (XRD), fourier transform infrared spectroscopy (FTIR) and temperature programmed desorption (TPD). The kinetic and thermodynamic performances of the $LiAlH_4$–TiF_3 composite will be further explored, and the in-situ formation of Al_3Ti in dehydrogenation will be discussed.

2. Experimental

The starting materials, $LiAlH_4$ (95%) were purchased from Acros Corp. and TiF_3 (99%) were purchased from Alfa Aesar. All the materials were used without further purification. $LiAlH_4$ was mechanically milled with x mol % (x = 1, 2, 4, 6) TiF_3 for 0.5 h under 1 MPa H_2 atmosphere using a QM-3SP2 planetary ball mill at 300 rpm in a stainless steel vessel. The ball-to-powder ratio was 60:1. For comparison, pure $LiAlH_4$ was also mechanically milled under identical conditions. All sample operations were performed in a glove box under Ar (99.999% purity) and the H_2O and O_2 contents were kept below 1 ppm.

XRD analysis was carried out using a powder X-ray Diffraction (XRD, Rigaku D/Max PC2500, Cu K_α radiation, 40 kV, 100 mA) at a scanning rate of 4° per min over the range of 20–80°2θ. The sample holder was covered with Mylar film to protect the sample from moisture and atmospheric oxygen during transportation. Temperature Programmed Desorption (TPD) of H_2 was performed using a home-made apparatus, which measures gas release rate at various temperatures. About 70 mg sample was used and heated at a ramping rate of 2 °C min^{-1} in a 35 mL/min Ar flow while heating from 30 to 260 °C. Dehydrogenation kinetics was measured by pressure-composition-temperature (PCT) apparatus at certain temperatures. FTIR spectra were measured by using an FTIR-650 spectrometer (Tianjin Gangdong) at a resolution of 4 cm^{-1}. Differential scanning calorimetry (DSC) was performed using a TA apparatus (DSC Q20P) in a flow (50 ml min^{-1}) of high purity Ar, with about 6 mg sample for each measurement.

3. Results and discussion

3.1. Dehydrogenation properties

3.1.1. Effect of the doping ratios on dehydrogenation

Firstly, the $LiAlH_4$-xTiF_3 composites (x = 0, 1, 2, 4, 6 mol %, respectively) have been prepared to optimize the addition amount of TiF_3, with x standing for the mole percentage of TiF_3 relative to $LiAlH_4$. For comparison, the dehydrogenation profiles of the doped samples and as-received $LiAlH_4$ are all presented in Fig. 1(A). Obviously, TiF_3 enormously enhances the dehydrogenation kinetics of commercial $LiAlH_4$. The dehydrogenation rate becomes faster with the adding amount of TiF_3 increasing. As shown from profile 'a' in Fig. 1(A), dehydrogenation of the undoped-$LiAlH_4$ sample occurs obviously in two steps (R1 and R2) and releases 7.4 wt % H_2 within 30 min at 250 °C. For comparison, $LiAlH_4$-1 mol % TiF_3 releases 6.96 wt % H_2 within 20 min; $LiAlH_4$-2 mol % TiF_3 releases 7.25 wt % H_2 within 18 min; $LiAlH_4$-4 mol% TiF_3 releases 6.82 wt % H_2 within 13 min; $LiAlH_4$-6 mol % TiF_3 releases 6.16 wt % H_2 within 10 min. As we can see, with increasing addition amount of TiF_3, dehydrogenation rate of $LiAlH_4$ increases considerably.

In contrast to the dehydrogenation rate, the H_2 release amount of $LiAlH_4$ decreases and is lower than that of the as-received $LiAlH_4$. We think that TiF_3 is a beneficial catalyst and effectively improves the dehydrogenation kinetics of pure $LiAlH_4$. As seen in Fig. 1(B), our initial speculation has been verified that more addition of TiF_3 further reduces the amount of released hydrogen when the H_2 capacity is calculated on the basis of the total mass of samples. Taking the dehydrogenation kinetics and hydrogen capacity into consideration, the $LiAlH_4$-2 mol % TiF_3 composite is the best compromise to be further explored.

Fig. 2 shows FTIR spectra of the 0.5 h ball-milled $LiAlH_4$ doped with 0, 1, 2, 4, 6 mol % TiF_3. For the undoped-$LiAlH_4$, the peaks at 883 and 705 cm^{-1} are the bending modes of $[AlH_4]^-$, and the peaks at 1780 and 1621 cm^{-1} are the stretching modes of $[AlH_4]^-$. There is no vibration peak of Li_3AlH_6. Thus, we can consider that as-milled $LiAlH_4$ is stable and no Li_3AlH_6 formed during ball milling. In comparison with the as–milled $LiAlH_4$, it is obvious that the $[AlH_4]^-$ bands for the $LiAlH_4$–TiF_3 composite are still in the same positions, however the peak intensities decrease. Obviously, there are IR vibration peaks (v_3 $[AlH_6]^{3-}$) at 1402 and 1298 cm^{-1} which are the stretching modes of $[AlH_6]^{3-}$, suggesting that a certain amount of $LiAlH_4$ decomposes into Li_3AlH_6, resulting from a small amount of hydrogen release during ball-milling. This is in accordance with the results of PCT that the hydrogen capacity of $LiAlH_4$–TiF_3 composite is lower than the as-received $LiAlH_4$ after ball–milling. As we can see, the stretching modes of $[AlH_6]^{3-}$ are weak, indicating a small amount of Li_3AlH_6. That is to say, only a small part of $LiAlH_4$ decomposes during high-energy ball milling process. Obviously, the peak intensity of the $[AlH_6]^{3-}$ increases with the content of TiF_3, indicating that the decomposition amount of $LiAlH_4$ increases. The addition of TiF_3 benefits reaction (R1) for $LiAlH_4$ during the ball milling.

3.1.2. Effect of placing for different time and temperature

As reported in literature, the initial temperature of $LiAlH_4$-4 mol % TiF_3 composites after ball milling is 80 °C [28]. However a special phenomenon was found in our experimental process, the decomposition amount of $LiAlH_4$ obviously decreased, after the ball-milled materials were placed at room temperature for a period of time. As shown in Fig. 3(A), if we make the dehydrogenation test of

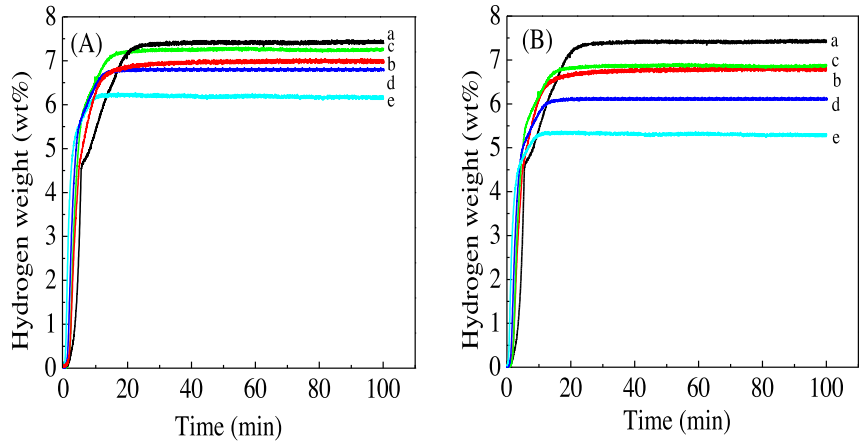

Fig. 1. The dehydrogenation profiles of the ball-milled $LiAlH_4$-xTiF_3 composites by PCT at 250 °C: (a) undoped-$LiAlH_4$; (b) $LiAlH_4$-1 mol % TiF_3; (c) $LiAlH_4$-2 mol % TiF_3; (d) $LiAlH_4$-4 mol % TiF_3; (e) $LiAlH_4$-6 mol % TiF_3. The hydrogen capacity was calculated: (A) only on the basis of $LiAlH_4$ and (B) after taking the weight of TiF_3 into account.

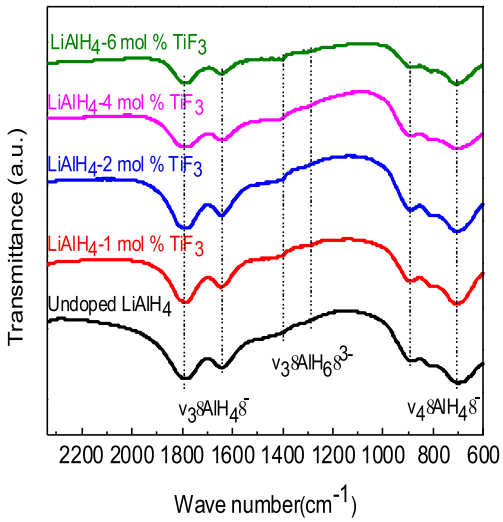

Fig. 2. FTIR spectra of the as-milled $LiAlH_4$; $LiAlH_4$-1 mol % TiF_3, $LiAlH_4$-2 mol % TiF_3, $LiAlH_4$-4 mol % TiF_3, $LiAlH_4$-6 mol % TiF_3 samples after ball milling.

the $LiAlH_4$-2 mol % TiF_3 composites at 250 °C immediately after ball milling, it releases 7.25 wt % H_2; however, the amount of H_2 release decreases to 7.04 wt % after the ball-milled sample is placed in the glove box for 5 h. This suggests that the sample probably releases some hydrogen when placed at room temperature. We then make the dehydrogenation test of samples which are placed in the glove box at room temperature (about 30 °C) for 10 h, 24 h, 48 h, and 120 h; and the amount of H_2 release is 6.32 wt %, 4.7 wt %, 3.87 wt % and 3.5 wt % respectively.

It would be reasonable that low temperature is beneficial to keep the samples from decomposition. As seen from profile 'a' in Fig. 4, the amount of hydrogen release from the sample kept at 0 °C for 48 h is 7.2 wt %, and it is almost the same as that from the as-prepared sample. For comparison, the amount of hydrogen release from the sample kept at room temperature (about 30 °C) for 48 h decreases to 4.3 wt %. We think that the $LiAlH_4$-2 mol % TiF_3 composites release hydrogen considerably at room temperature. With the addition of TiF_3 catalyst, the initial dehydrogenation temperature of $LiAlH_4$ reduces to nearly room temperature. The XRD tests have provided evidence for this explanation. As shown in Fig. 3 (B), the peak at $2\theta = 31.6$ belongs to the Li_3AlH_6. The diffraction intensity of Li_3AlH_6 is stronger with increasing time of placing at room temperature; meanwhile, the peak intensity of Al is

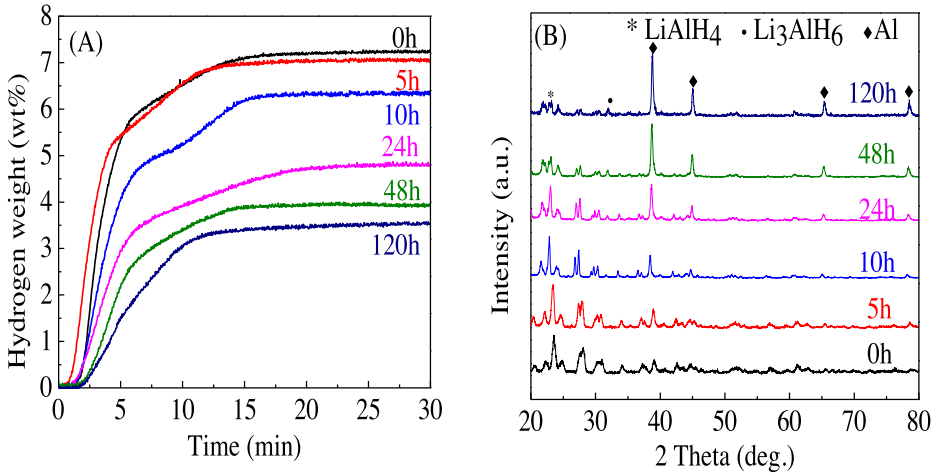

Fig. 3. (A) The dehydrogenation profiles and (B) The XRD profiles of the ball-milled $LiAlH_4$-2 mol % TiF_3 composites placed in the glove box for different lengths of time at room temperature.

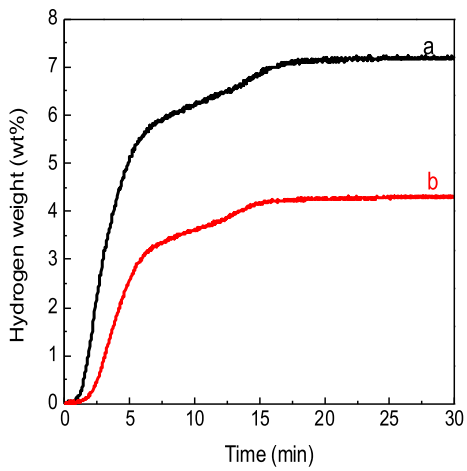

Fig. 4. The dehydrogenation profiles at 250 °C of the ball-milled $LiAlH_4$-2 mol % TiF_3 composites (a) kept with ice bath at 0 °C; (b) placed in the glove box at room temperature for 48 h, respectively.

stronger and the peak of $LiAlH_4$ decreases. The first reaction (R1) of $LiAlH_4$-2 mol % TiF_3 composites takes place at room temperature.

3.1.3. TPD measurements

TPD tests further prove our speculation. Fig. 5 shows TPD curves of the ball-milled $LiAlH_4$ doped with 0, 1, 2, 4, 6 mol % TiF_3. As shown in Fig. 5(A), there are two distinct hydrogen desorption peaks for five samples when heating from 30 °C to 260 °C, which is in accordance with the two-step dehydrogenation reaction (R1 and R2) of $LiAlH_4$. The onset temperature of the undoped-$LiAlH_4$ sample is around 145 °C with the maximum at 179.9 °C. The $LiAlH_4$-2 mol % TiF_3 sample starts to release hydrogen at around 35 °C with the maximum at 108.4 °C, which is 71.5 °C lower than that for the undoped-$LiAlH_4$ sample (179.9 °C). It has proved that the onset temperature of $LiAlH_4$-2 mol % TiF_3 composites has reduced to nearly room temperature. Furthermore, the peak of dehydrogenation shifts to lower temperatures with TiF_3 amount increasing. The peak of the first reaction for $LiAlH_4$–TiF_3 is a broad peak. For the second dehydrogenation reaction, the signal intensities become weaker with increasing TiF_3 amount, and the dehydrogenation temperature just decreases a little. It is clear that TiF_3 is an effective catalyst for the decrease of desorption temperature.

Fig. 5(B) presents the TPD dehydrogenation capacity of $LiAlH_4$, $LiAlH_4$-1 mol % TiF_3, $LiAlH_4$-2 mol % TiF_3, $LiAlH_4$-4 mol % TiF_3 and $LiAlH_4$-6 mol % TiF_3. The dehydrogenation capacity decreases with increasing addition amount of TiF_3 from 1 to 2 mol %, and then it decreases from 2 to 6 mol %. It reveals that the hydrogen capacity reduces obviously with more addition of TiF_3. TiF_3 catalyst decreases the dehydrogenation temperature, with the cost of loss of hydrogen release content. The excessive amount of TiF_3 catalyst is detrimental for hydrogen capacity. The hydrogen desorption capacity of $LiAlH_4$-2 mol %TiF_3 sample is 7.1 wt %, which is more than those of any other doping samples. The doping of TiF_3 is beneficial for complete decomposition of $LiAlH_4$ which leads to an increase of hydrogen capacity. On the other hand, the loss of hydrogen probably increases with more TiF_3 during ball milling, which then leads to a decrease of hydrogen capacity. As a result of the two factors, the hydrogen capacity of $LiAlH_4$-2 mol % TiF_3 composite reaches a maximum. However, the hydrogen capacity of doped-$LiAlH_4$ samples is always lower than the theoretical value (7.9 wt %). It is because as-received $LiAlH_4$ sample containing impurities, which results in the hydrogen capacity not reaching the theoretical value. On the other hand, the TiF_3 also makes $LiAlH_4$ decompose to Li_3AlH_6 and release a small amount of hydrogen during ball-milling, which has been confirmed by the IR spectra. Meanwhile, R1 becomes slower and goes on over a wider temperature range and the boundaries of R1 and R2 becomes more and more undefined, it is probably because R2 already starts before R1 finishes completely [28]. The details of TPD dehydrogenation curves are shown in Table 1.

3.2. Dehydrogenation kinetics and thermodynamics

The dehydrogenation kinetics of the $LiAlH_4$-2 mol % TiF_3 sample under relatively lower temperatures are shown in Fig. 6, while the kinetic behavior of undoped-$LiAlH_4$ is also included. The results show that the $LiAlH_4$-2 mol % TiF_3 composite releases 1.75, 3.25, 4.1, 5.1, 6.77 and 7.0 wt % H_2 at 45, 60, 80, 100, 120 and 140 °C, respectively. The hydrogen capacity becomes higher with higher desorption temperatures. Acting as a catalyst, TiF_3 enormously decreases the dehydrogenation temperature. As can be seen from Fig. 6, at 140 °C, the $LiAlH_4$-2 mol % TiF_3 sample releases 7 wt % H_2 within 80 min, whereas the undoped $LiAlH_4$ sample (without ball milling) only releases 0.8 wt % H_2 within the same time. The hydrogen capacity of the undoped $LiAlH_4$ is only 4.4 wt % at this temperature. At 45 °C, the $LiAlH_4$-2 mol % TiF_3 sample releases about 1.75 wt % H_2 within 8 h; on the other hand, the undoped sample cannot release H_2 at this temperature. The above results show that the dehydrogenation rate of $LiAlH_4$-2 mol % TiF_3 is much faster than that of the undoped $LiAlH_4$. The improved kinetics is

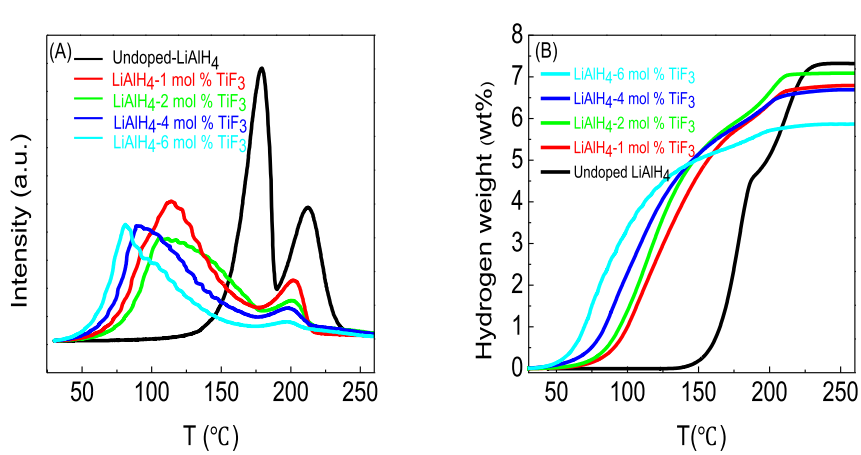

Fig. 5. TPD dehydrogenation curves of undoped-$LiAlH_4$, $LiAlH_4$-1 mol % TiF_3, $LiAlH_4$ – 2 mol % TiF_3, $LiAlH_4$-4 mol % TiF_3, $LiAlH_4$-6 mol % TiF_3 (Heating ramp 2 °C/min).

Table 1
Details of TPD dehydrogenation curves of undoped-$LiAlH_4$, $LiAlH_4$-1 mol % TiF_3, $LiAlH_4$-2 mol % TiF_3, $LiAlH_4$-4 mol % TiF_3, $LiAlH_4$-6 mol % TiF_3.

	Initial temp. (°C)	Dehydrogenation peak of R_1 (°C)	Dehydrogenation peak of R_2 (°C)	Total amount of H_2 release (%)
$LiAlH_4$	145	179.9	216.6	7.3
$LiAlH_4$-1 mol % TiF3	35	114.6	202.2	6.8
$LiAlH_4$-2 mol % TiF3	35	108.4	201.9	7.1
$LiAlH_4$-4 mol % TiF3	35	88.1	198	6.7
$LiAlH_4$-6 mol % TiF3	35	80.5	194	5.9

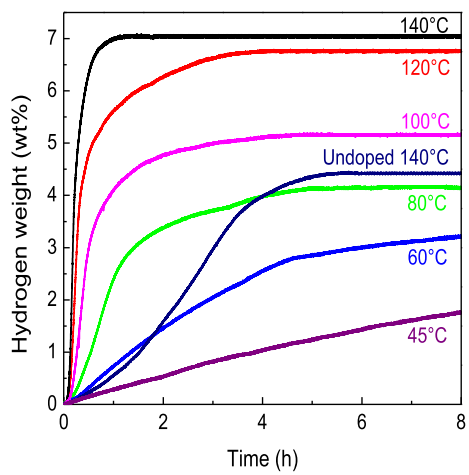

Fig. 6. The PCT dehydrogenation characteristics of undoped $LiAlH_4$ sample at 140 °C and ball-milled $LiAlH_4$-2 mol % TiF_3 sample at various temperatures.

probably owing to the defect creation, formation of some kind of active material, and particle size reduction during milling [28,42–44]. Moreover, the catalytic properties of TiF_3 is superior to some previously documented catalysts, such as $TiCl_4$ [20], elemental metals [22–25], carbon material [34,36].

To further investigate dehydrogenation kinetics and thermodynamics of $LiAlH_4$-2 mol % TiF_3 sample, the DSC curves were measured with heating from 50 °C to 260 °C at various rates of 2, 5, 8 °C/min, respectively. In the aspect of thermodynamics, as shown in Fig. 7 (A), DSC curves of $LiAlH_4$-2 mol % TiF_3 sample exhibit two distinct endothermic peaks at heating ramp of 2 °C/min. Clearly, the first peak of $LiAlH_4$-2 mol % TiF_3 sample is at about 125.81 °C and the second is at 179.83 °C, which corresponds to the two-step decomposition reactions. To explore how the TiF_3 catalyst acts on the kinetic performance of $LiAlH_4$, Ea of $LiAlH_4$-2 mol % TiF_3 sample has been determined with the Kissinger's approach [16]. Fig. 7(B) shows the Arrhenius plots for the two endothermic peaks of $LiAlH_4$-2 mol % TiF_3 sample. Ea of the two dehydrogenation reactions for $LiAlH_4$ is deduced to be 66.76 kJ mol^{-1} and 88.21 kJ mol^{-1}, which are 49.44 kJ mol^{-1} and 44.79 kJ mol^{-1} lower than the theoretical value of pure $LiAlH_4$ (116.2 kJ mol^{-1} and 133.0 kJ mol^{-1}) [35]. This reveals that the TiF_3 enormously reduces the activation energy of $LiAlH_4$ and obviously improves the dehydrogenation kinetics of $LiAlH_4$-2 mol % TiF_3 composite.

3.3. Mechanism analysis

Fig. 8 shows the XRD patterns of as-received $LiAlH_4$, as-milled $LiAlH_4$, as-milled $LiAlH_4$-2 mol % TiF_3 and $LiAlH_4$-2 mol % TiF_3 after dehydrogenation. The small peak at $2\theta = 34.8$ is the impurity LiCl, which could explain the results of PCT and TPD that the dehydrogenation capacity of doping $LiAlH_4$ is lower than theoretical capacity. As seen from profile 'b' in Fig. 8, the peak positions of as-milled $LiAlH_4$ were the same as those of the as-received $LiAlH_4$ except for the decreasing of intensity. That is to say, ball-milling does not make $LiAlH_4$ decompose and just make the particle size smaller. As seen from profile 'c', the small peak at $2\theta = 31.6$ belongs to the Li_3AlH_6. A small amount of $LiAlH_4$ has already decomposed to Li_3AlH_6, which is consistent with the result of FTIR. However, it should be noted that no F-containing and Ti-containing phases are detected after ball milling or after dehydrogenation. It is probably because that their amount is beyond the detection limit of XRD technique or it is in amorphous state. The following reactions probably take place, according to the mechanism proposed by S.-S. Liu et al. [28].

$$3LiAlH_4 + TiF_3 \rightarrow 3LiF + Al_3Ti + 6H_2 \quad \text{R4}$$

$$3LiAlH_4 + TiF_3 \rightarrow 3LiF + 3Al + TiH_2 + 5H_2 \quad \text{R5}$$

$$3LiAlH_4 + TiF_3 \rightarrow 3LiF + 3Al + Ti + 6H_2 \quad \text{R6}$$

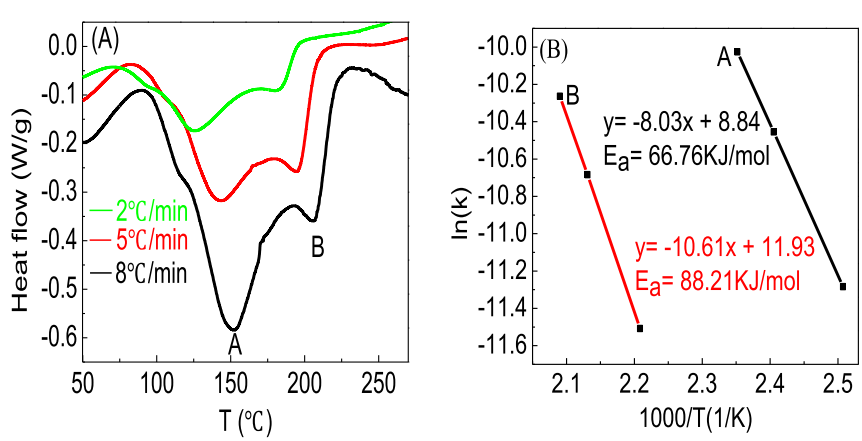

Fig. 7. (A) DSC profiles of $LiAlH_4$-2 mol % TiF_3 sample(2, 5 and 8 °C min^{-1}); (B) Kissinger plots for the dehydrogenation of $LiAlH_4$-2 mol % TiF_3 sample (A: $LiAlH_4 \rightarrow Li_3AlH_6$; B: $Li_3AlH_6 \rightarrow LiH$).

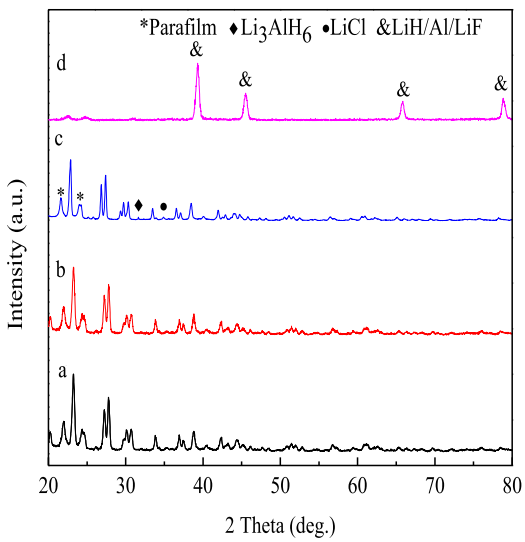

Fig. 8. XRD patterns of the samples (a) as-received $LiAlH_4$; (b) as-milled $LiAlH_4$; (c) as-milled $LiAlH_4$-2 mol % TiF_3; (d) $LiAlH_4$-2 mol % TiF_3 after dehydrogenation.

Kang et al. conclude that the formation of Al_3Ti is favorable. Because Al_3Ti (ΔG_f.136 kJ mol^{-1}) is more stable than TiH_2 (ΔG_f.86 kJ mol^{-1}) [45]. It is thought that only some of TiF_3 reacted with $LiAlH_4$ to form the catalyst Al_3Ti during ball-milling and Al_3Ti catalyzed the $LiAlH_4$ decomposition to Li_3AlH_6. However, Al_3Ti is not detected after dehydrogenation. It is probably because the diffractions of Al_3Ti are weak due to its large peak widths, high dispersion, some amorphous state or small amount [46]. However, another view indicates that fluorine substitute hydrogen to form the stable structures of AlF_6^- and AlF_4^-, which tends to facilitate hydrogen desorption [39–41].

To further investigate catalytic mechanism of TiF_3, the PCT and XRD curves were measured with the $LiAlH_4$–TiF_3 samples of 3:1 mol ratio. As seen from profile 'b' in Fig. 9(A), the $3LiAlH_4$–TiF_3 sample with physical mixture quickly releases nearly 9 wt % H_2 (larger than 7.9 wt %, which is the sum of hydrogen release from R1 and R2) within 2 min at 250 °C. Correspondingly, the diffraction peaks of Al_3Ti and LiF are present in profile 'd' in Fig. 9(B). Although the formation of Al_3Ti has been confirmed during the process of ball milling [37,38], the Al_3Ti formed in-situ during dehydrogenation process has been detected by XRD for the first time to our best knowledge. Thus, we can believe that $LiAlH_4$ reacts with TiF_3 as reaction R4, not R5 or R6, and Al_3Ti forms in the process of dehydrogenation when the ratio is 3:1 at certain temperatures; and the in-situ formed Al_3Ti catalyzes dehydrogenation through reaction R1 and R2. However, the dehydrogenation capacity cannot reach the theoretical value (10.5 wt %), it is probably because the as-received $LiAlH_4$ is not pure and some $LiAlH_4$ still decomposes as R1 and R2, which lowers the dehydrogenation capacity of the samples.

For comparison, the ball-milled sample releases only 2.2 wt % H_2 at 250 °C, and Al_3Ti cannot be found in the XRD patterns both before and after dehydrogenation. However, there was a small amount of $LiAlH_4$ remaining after ball milling. We can deduce that only a small amount of $LiAlH_4$ reacts with TiF_3 as R4 during ball milling even though the ratio is 3:1. It is probably because the slow speed and the small energy of ball milling could not make the reaction complete. And then the formed Al_3Ti catalyzes the $LiAlH_4$ decompose, whereas the amount of Al_3Ti is still beyond the detection limit of XRD, or it is amorphous in the samples. From the results above, we can verify the formation of crystalline Al_3Ti in reaction R4.

4. Conclusions

It has been demonstrated that TiF_3 obviously enhances the desorption kinetics of as-received $LiAlH_4$. The addition of 2 mol % TiF_3 leads to the onset temperature of $LiAlH_4$ decreasing to around 35 °C and the dehydrogenation rate reaches a maximum value at 108.4 °C. As for the dehydrogenation kinetics, the $LiAlH_4$-2 mol % TiF_3 sample releases about 7.0 wt % H_2 at 140 °C within 80 min. The Ea values of the $LiAlH_4$-2 mol % TiF_3 sample decrease to 66.76 kJ mol^{-1} and 88.21 kJmol^{-1} for the two hydrogen desorption reaction of $LiAlH_4$, resulting in a faster dehydrogenation rate. The presence of Li_3AlH_6 is confirmed by FTIR and XRD after ball milling, demonstrating that the addition of TiF_3 leads to the decomposition of $LiAlH_4$ during ball milling. On reaction mechanism, the in-situ formed Al_3Ti has been found in XRD patterns of the mixed $3LiAlH_4$–TiF_3 samples without ball milling, after dehydrogenation at 250 °C. TiF_3 presumably reacts with $LiAlH_4$ to form the Al_3Ti and LiF, following the proposed reaction R4, and then the formed Al_3Ti catalyzes $LiAlH_4$ to decompose.

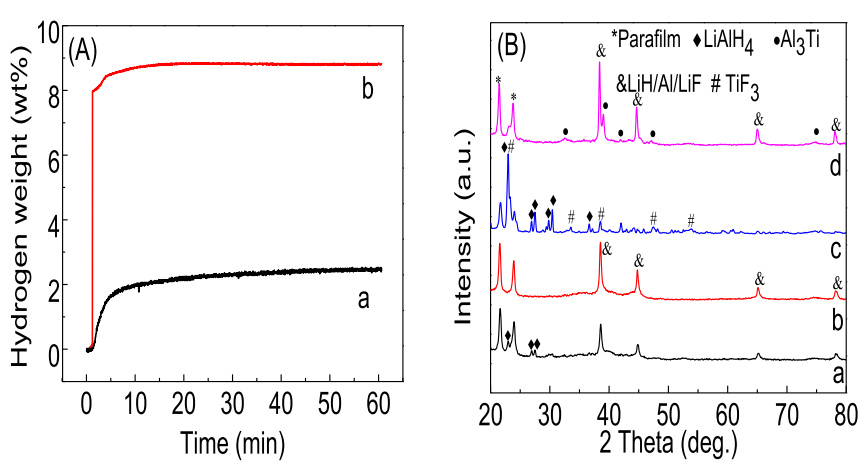

Fig. 9. (A) PCT profiles of $3LiAlH_4$–TiF_3 sample at 250 °C (a: after ball milling; b: physical mixture without ball milling); (B) XRD profiles of $3LiAlH_4$–TiF_3 sample (a: the ball-milled sample before dehydrogenation, b: the ball-milled sample after dehydrogenation; c: the physically-mixed sample before dehydrogenation, d: the physically-mixed sample after dehydrogenation).

Acknowledgment

The authors thank the Tianjin Natural Science Foundation 09JCZDJC24800 for the financial support for our research.

References

[1] M.Q. Fan, S. Liu, L.X. Sun, F. Xu, S. Wang, J. Zhang, D.S. Mei, F.L. Huang, Q.M. Zhang, Int. J. Hydrogen Energy 37 (2012) 4571–4579.
[2] H.B. Dai, G.L. Ma, H.J. Xia, P. Wang, Energy & Environ. Sci. 4 (2011) 2206–2212.
[3] K.A. Brown, S. Dayal, X. Ai, G. Rumbles, P.W. King, J. Am. Chem. Soc. 28 (2010) 9672–9680.
[4] K.M. Fair, X.Y. Cui, L. Li, C.C. Shieh, R.K. Zheng, Z.W. Liu, B. Delley, M.J. Ford, S.P. Ringer, C. Stampfl, Phys. Rev. B 87 (2013) 014102.
[5] J. Hensel, G. Wang, Y. Li, J.Z. Zhang, Nano Lett. 2 (2010) 478–483.
[6] D. Streich, Y. Astuti, M. Orlandi, L. Schwartz, R. Lomoth, L. Hammarstrom, S. Ott, Chem. A Euro. J. 1 (2010) 60–63.
[7] Z.G. Huang, T. Autrey, Energy Environ. Sci. 5 (2012) 9257–9268.
[8] R. Khnayzer, L.B. Thompson, M. Zamkov, S. Ardo, G. Meyer, C. Murphy, F.N. Castellano, J. Phys. Chem. C 1 (2012) 1429–1438.
[9] H.M. Chen, C.K. Chen, M.L. Tseng, P.C. Wu, C.M. Chang, L.C. Cheng, H.W. Huang, T.S. Chan, D.W. Huang, R.-S. Liu, Small 17 (2013) 2926–2936.
[10] D.J. Bull, E. Weidner, I.L. Shabalin, M.T.F. Telling, C.M. Jewell, D.H. Gregory, D.K. Ross, Phys. Chem. Chem. Phys. 12 (2010) 2089–2097.
[11] H. Lv, J. Song, H. Zhu, Y.V. Geletii, J. Bacsa, C. Zhao, T. Lian, D.G. Musaev, C.L. Hill, J. Catal. 307 (2013) 48–54.
[12] B. Johnston, M.C. Mayo, A. Khare, Technovation 25 (2005) 569–585.
[13] S. Satyapal, J. Petrovic, C. Read, G. Thomas, G. Ordaz, Catal. Today 120 (2007) 246–256.
[14] L. Li, Y. Wang, F.Y. Qiu, Y.J. Wang, Y.N. Xu, C.H. An, L.F. Jiao, H.T. Yuan, J. Alloy Compd. 566 (2013) 137–141.
[15] R.A. Varin, L. Zbroniec, J. Alloy Compd. 504 (2010) 89–101.
[16] A. Andreasena, T. Veggea, A.S. Pedersena, J. Phys. Chem. C 116 (2012) 22327–22335.
[17] F.Q. Zhai, P. Li, A.Z. Sun, S. Wu, Q. Wan, W.N. Zhang, Y.L. Li, L.Q. Cui, X.H. Qu, J. Phys. Chem. C 116 (2012) 11939–11945.
[18] J. Chen, N. Kuriyama, J. Phys. Chem. B 105 (2001) 11214–11220.
[19] P. Li, Z.L. Li, F.Q. Zhai, Q. Wan, X.Q. Li, X.H. Qu, A.V. Alex, J. Phys. Chem. C 117 (2013) 25917–25925.
[20] V.P. Balema, J.W. Wiench, K.W. Dennis, J. Alloy Compd. 329 (2001) 108.
[21] T. Czujko, Z. Zaranski, I.E. Malka, Z. Wronski, J. Alloys Compd. 509 (2011) 604–609.
[22] M. Resan, M.D. Hampton, J.K. Lomness, D.K. Slattery, Int. J. Hydrogen Energy 30 (2005) 1417–1421.
[23] H.W. Langmi, G.S. McGrady, X.F. Liu, C.M. Jensen, J. Phys. Chem. C 114 (2010) 10666–10669.
[24] A.V. Robert, R. Parviz, Int. J. Hydrogen Energy 37 (2012) 9088–9102.
[25] X.P. Zheng, X.H. Qu, I.S. Humail, P. Li, G.Q. Wang, Int. J. Hydrogen Energy 32 (2007) 1141–1144.
[26] D. Blanchard, H.W. Brinks, B.C. Hauback, P. Norby, Mater. Sci. Eng. B 108 (2004) 54–59.
[27] J.R. Ares, K.F. Aguey-Zinsou, M. Elsaesser, X.Z. Ma, M. Dornheim, T. Klassen, Int. J. Hydrogen Energy 32 (2007) 1033–1040.
[28] S.S. Liu, L.X. Sun, Y. Zhang, F. Xu, J. Zhang, H.L. Chu, M.Q. Fan, T. Zhang, X.Y. Song, J.P. Grolier, Int. J. Hydrogen Energy 34 (2009) 8079–8085.
[29] B.A. Placidus, T.G. John, J.S. Patrick, A.V. Andrey, S.F. Timothy, J. Phys. Chem. C 116 (2012) 21886–21894.
[30] J. Fu, L. Rontzsch, T. Schmidt, M. Tegel, T. Weißgarber, B. Kieback, Int. J. Hydrogen Energy 37 (2012) 13387–13392.
[31] Rafiuddin, X.H. Qu, P. Li, L. Zhang, A. Mashkoor, J. Phys. Chem. C 26 (2011) 13088–13099.
[32] Z.L. Li, P. Li, Q. Wan, F.Q. Zhai, Z.W. Liu, K.F. Zhao, L. Wang, S.Y. Lu, L. Zou, X.H. Qu, A. Alex, M. Volinsky, J. Phys. Chem. C 117 (2013) 18343–18352.
[33] R.A. Varin, R. Parviz, Int. J. Hydrogen Energy 39 (2014) 2575–2586.
[34] M. Ismail, Y.X. Zhao, B. Yu, S.X. Dou, Int. J. Electroact. Mater. 1 (2013) 13–22.
[35] Q. Wan, P. Li, Z.L. Li, F.Q. Zhai, X.H. Qu, A. Alex, J. Phys. Chem. C 117 (2013) 26940–26947.
[36] W.C. Hsu, C.H. Yang, W.T. Tsai, Int. J. Hydrogen Energy 39 (2014) 927–933.
[37] V.P. Balema, J.W. Wiencha, K.W. Dennisa, M. Pruskia, V.K. Pecharsky, J. Alloy Compd. 329 (2001) 108–114.
[38] E.H. Majzoub, K.J. Gross, J. Alloy Compd. 356 (2003) 363–367.
[39] N. Eigen, U. Boesenberg, J.B. von Colbe, J. Alloy Compd. 477 (2009) 76–80.
[40] L.H. Rude, U. Filsø, V. D'Anna, A. Spyratou, B. Richter, S. Hino, Phys. Chem. Chem. Phys. 15 (2013) 18185–18194.
[41] H.W. Brinks, A. Fossdal, B.C. Hauback, J. Phys. Chem. C 112 (2008) pp.5658–pp.5661.
[42] J.R. Ares, K.F. AgueyeZinsou, M. Porcu, J.M. Sykes, M. Dornheim, T. Klassen, Mater. Res. Bull. 43 (2008) 1263–1275.
[43] L.H. Kumar, B. Viswanathan, S.S. Murthy, Int. J. Hydrogen Energy 33 (2008) 366–373.
[44] L. Li, Y.N. Xu, Y. Wang, Y.J. Wang, F.Y. Qiu, C.H. An, L.F. Jiao, H.T. Yuan, Dalton Trans. 43 (2014) 1806–1813.
[45] X.D. Kang, P. Wang, X.P. Song, X.D. Yao, G.Q. Lu, H.M. Cheng, J. Alloy. Compd. 424 (2006) 365–369.
[46] S.S. Liu, Y. Zhang, L.X. Sun, J. Zhang, J.N. Zhao, F. Xu, F.L. Huang, Int. J. Hydrogen Energy 35 (2010) 4554–4561.